Observations of the blazar Markarian 501 using the VERITAS Čerenkov telescope array

William Gignac[1]

Department of Astronomy and Astrophysics, University of Chicago, Chicago, IL 60637

`wtgignac@uchicago.edu`

ABSTRACT

The blazar galaxy Markarian 501 has undergone extensive study since it became the second Active Galactic Nucleus to be detected as a source of very high energy γ-rays by a ground based γ-ray telescope in 1995. Since then, observers have found it to be a capricious source, with a γ-ray flux that ranges from hardly detectable levels to those making it the brightest γ-ray source in the sky. At the lower end of this spectrum, the sensitivity of the first-generation Čerenkov imaging telescopes has inhibited observers from fully characterizing the γ-ray signal. Presented here are results of observations of Markarian 501 using the newly constructed VERITAS two telescope array of next-generation Čerenkov imaging telescopes. A strong signal (7.57 σ) was detected after 11 hours of observation over the span of 2 months, while Markarian 501 was in a low emission state (0.13 γ-rays min^{-1}). These observations may be among the first extended detections of Markarian 501 in a low emission state, a promising step towards being able to characterize the blazar's quiescent emission behavior. Furthermore, the success at obtaining a significant detection from Markarian 501 in a low-level emission state is encouraging for the future completed VERITAS array and next gereneration Čerenkov telescope arrays in general.

1. Introduction

The BL Lacertae object Markarian 501 ($z = 0.034$) was first discovered as a source of very high energy gamma rays (E > 300 GeV) by the Whipple collaboration in 1995 as part of a search for high energy photo emission from active galactic nuclei (AGN) (Quinn et al. 1996). It had previously been shown that certain AGN known as *blazars* that have

---

[1]NSF REU Student at the University of California, Los Angeles, Los Angeles, CA 90095.

relativistic jets of charged particles aligned towards Earth could be a source of very energetic photons when the blazar Markarian 421 was detected by Whipple (Punch et al. 1992). The detection of Markarian 501, also a blazar, confirmed this observation. The rate of excess gamma-ray detection from Markarian 501 at these energies was 0.15 γ-rays min^{-1}, less than 20% of the rate from Markarian 421, and less than 10% of the rate from the Crab supernova remnant, making it one of the weakest detected gamma-ray sources in the sky. After 37.9 hours of observation, the detection had a significance of 8.36σ (where σ is one standard deviation above background detection level). The detection of Mrk 501 was subsequently confirmed by the HEGRA experiment at energies above 1.5 TeV, and was observed to have a similarly low excess gamma-ray detection rate of 2.5 γ-rays hr^{-1}, and a significance of 5.2σ after 146.8 hours of observation (Bradbury et al. 1997).

In April of 1997, observers saw a dramatic change in the gamma-ray flux from Mrk 501 as it flared to levels as much as six times greater than that of the Crab (Catanese et al. 1997; Aharonian et al. 1997). At such high emission rates, it became possible to measure variablility in the gamma-ray flux on short timescales (< 1 day), and it was seen that Mrk 501 displays rapid variability similar to that of Mrk 421 (Quinn et al. 1999). It appears, then that Mrk 501 has a base low-level emission state and undergoes periods of violent and variable flaring. While the behavior of the blazar has been extensivly studied during these periods of flaring, the sensitivity of the first-generation of Čerenkov imaging telescopes prevented an accurate characterization of its low level emission, particularly on timescales shorter than one day. These limitations will be overcome by the newly-constructed next-generation Čerenkov imaging telescope arrays H.E.S.S., MAGIC, and VERITAS. Thus far, the H.E.S.S. telescope has found only a small signal from Mrk 501 at its low level state. After 1.8 hours of observation, the H.E.S.S. collaboration detected Mrk 501 with a significance of 3.1σ and a flux 15% of that of the Crab Nebula at energies $E > 1.65$ TeV (Aharonian et al. 2005). The MAGIC experiment has only detected Mrk 501 at a high level of emission (Rico & the MAGIC collaboration 2006). What follows is a presentation of observations of Mrk 501 by the VERITAS Čerenkov imaging array in its current, two telescope state.

2. The VERITAS Telescope Array

The VERITAS atmospheric Čerenkov imaging telescopes are currently located at the base of Mt. Hopkins, the site of the Whipple Observatory, in southern Arizona. Upon completion in early 2007, the VERITAS system will consist of an array of four telescopes, but at this time only two of the telescopes have been constructed. This two telescope system has taken a few months of stereoscopic data during the first half of 2006, and will resume

data collection after the end of the summer monsoon season.

Each telescope in the array is of Davies-Cotton architecture (Davies & Cotton 1957), with a 12 m aperture spherical reflector with a 12 m focal length (see Figure 1). The reflector consists of 350 identical hexagonal mirrors, each with radius of curvature 24 m $\pm$ 1%, mounted on a steel Optical Support Structure (OSS). The mirrors are designed to have > 90% reflectivity at the peak Čerenkov light wavelength of 320 nm. Located at the focus of the reflector is a high resolution, 499 pixel photomultiplier tube (PMT) camera with a total field of view diameter of approximately 3.5° (see Figure 2).

During observation, the reflector focuses light onto the PMT camera, producing a voltage signal in each PMT that is subsequently digitized using a 500 MHz flash-ADC system and stored in memory buffers. In order to recognize potential Čerenkov shower images, each VERITAS telescope is equipped with pixel-level and telescope-level triggers. For each pixel, the pixel-level trigger requires that the charge within the pixel channel exceed a certain threshold. For the data presented below, this threshold was $\sim 4 - 5$ photoelectrons. When this threshold is exceeded, the pixel-level trigger sends a pulse to the telescope-level trigger system. At this level, it is determined whether or not within a short timeframe (~ 6 ns) the triggered pixels have a predetermined topology. The topology is chosen to reduce the number of triggers due solely to night sky light fluctuations. Currently VERITAS requires that three adjacent pixels be triggered. If the telescope-level trigger is satisfied, fast signals are sent to the central location where the array trigger decision is made. The array trigger requires both telescope trigger signals, appropriately delayed, to overlap in time in a window of ~ 60 ns width. If this condition is satisfied, the array trigger signals each telescope to store the FADC information for that event. The data from the two telescopes are merged to form array events on the central Harvester CPU. For a more detailed description of the VERITAS array system, see Holder et al. (2006).

3. Data Analysis

The data presented here were collected over 14.5 hr. during the course of eleven nights between April 26 and June 19 of 2006. Data collection consisted of ~ 28 minute observation runs, meant to be analyzed using the wobble analysis technique (described below), so the telescopes were pointing slightly off source, usually approximately $\pm 0.3°$ in either right ascension (RA) or declination (Dec). Of the total 31 observation runs, 7 were unanalyzable due to observer and hardware error, so a net total of 24 observation runs (11 hr.) are presented in the following analysis (see Table 1).

3.1. Calibration

In order to analyze the images stored during the observation runs, it is first necessary to account for the hardware dependency of the images. Each PMT, for example, will have a different base DC level or pedestal, which, though stored in the recorded images, should not be considered as part of the signal due to Čerenkov shower light. To determine the magnitude of these pedestals, the array is triggered at a fixed frequency (3 Hz) during the observation run and thecamera images are read out as usual. These pedestal events are then usedto determine the pedestal level for each PMT channel. In subsequent stages of analysis, this pedestal is subtracted from the image's PMT charges (See Figures 3 and 4). Also calculated is the variance σ of the PMT charge around this pedestal level. As the small fluctuations around the pedestal are due primarily to small fluctuations in background light and other noise, σ is a measurement of the total noise in the PMT.

It is also necessary to take into account the differences in the individual PMT gains. To determine the gains of each of the PMTs, during every night of observation a calibration run is performed, in which a nitrogen laser sends a short (4 ns) pulse into a dye module, which in turn fluoresces, giving light that is used to uniformly illuminate the telescope camera (Holder et al. 2006). From the response of each of the PMTs, their relative gains may be calculated; this information is then used to scale the charge in each PMT so as to equalize the gains during data analysis (See Figure 5).

3.2. Image Cleaning

After the hardware dependency of the images has been removed, what remains is an image that accurately reflects the light recorded during the potential gamma-ray event. Not all of the light recorded comes from a Čerenkov shower, however. In order to consider only pixels that detected light from a Čerenkov shower rather than simply night sky noise, a cleaning algorithm is employed to remove pixels from the image that are consistent with being noise. To quantify this, for each pixel we calculate the signal-to-noise ratio η. For the kth pixel, η_k is defined as

$$\eta_k = \frac{q_k}{\sigma_k} \tag{1}$$

where q_k is the charge in the pixel. If $\eta_k > 5$, then the channel information is kept. Further, if $\eta_k > 3$ and the kth pixel is adjacent to a jth pixel with $\eta_j > 5$, then the channel information is kept. This second criterion is designed to keep information from pixels on the boundary of a shower image. All other channels have their information discarded. The result of such cleaning can be seen in Figure 6.

3.3.   Image Parameterization

The images produced by the previous stages reflect as accurately as possible the light detected from a potential Čerenkov shower. The vast majority of the Čerenkov showers detected will be due to cosmic rays rather than gamma rays, so it is necessary to employ an algorithm to preferentially select gamma-ray shower images and reject background hadronic shower images. Since experience and simulations have told us that gamma-ray shower images tend to be more compact and elliptical while cosmic ray shower images are larger and more chaotic, to reject the hadronic background it is necessary to quantify the dimensions of the image. The next stage in the data analysis, image parameterization, performs a moment analysis on the image to do precisely this. For each camera image recorded for every telescope in the array, the following procedure is used. First, the zeroth order moment S^0, or image *size*, is calculated as

$$S^0 = \sum_{k=1}^{N_{chan}} q_k. \tag{2}$$

This is then simply a measure of the total light in the image. The first order moments S^1_i ($i = 1, 2$) are then calculated as

$$S^1_i = \sum_{k=1}^{N_{chan}} q_k x_{ik} \tag{3}$$

where x_{ik} is the x_ith coordinate of the kth pixel, measured from the camera center. The first order moment is used to determine the centroid of the image $(\overline{x_1}, \overline{x_2})$

$$\overline{x_i} = \frac{S^1_i}{S^0} \tag{4}$$

from which the *distance d* of the image from the camera center is calculated:

$$d = \sqrt{\overline{x_1}^2 + \overline{x_2}^2} \tag{5}$$

The second order moments S^2_{ij} ($i, j = 1, 2$) are calculated as

$$S^2_{ij} = \sum_{k=1}^{N_{chan}} q_k \left(x_{ik} - \overline{x_i}\right) \left(x_{jk} - \overline{x_j}\right) \tag{6}$$

The second order moment matrix $\mathbf{X^2} = \left(S^2_{ij}/S^0\right)$ has eigenvalues ℓ^2 and w^2 which can be obtained via conjugation with a rotation matrix:

$$\mathbf{X^2} = \begin{pmatrix} \cos\beta & \sin\beta \\ -\sin\beta & \cos\beta \end{pmatrix} \begin{pmatrix} \ell^2 & 0 \\ 0 & w^2 \end{pmatrix} \begin{pmatrix} \cos\beta & \sin\beta \\ -\sin\beta & \cos\beta \end{pmatrix}^{-1} \tag{7}$$

Finding the parameters ℓ, w, and β gives us the length, width, and orientation of an elliptical approximation of the image (see Figures 7 and 8).

3.4. Shower Reconstruction

With the image parameters calculated, one can reconstruct the shower direction as well as the extrapolated impact position of the shower's core with the ground (the *core position*). A simple geometric method is used to determine both of these. To determine the shower direction, the ellipses fit to the shower images from each telescope are superimposed onto the field of view of the telescope as shown in Figure 8. Because the ellipses tend to point back to the direction from which the shower started, intersecting the major axes of the ellipses gives the position in the sky where the shower started. Similarly, by projecting the images on the ground coordinate plane, we can reconstruct the point of impact of the shower core (see Figure 9).

Ultimately, to determine whether or not the source being observed is a gamma-ray source, one needs to determine if the gamma rays detected by the telescope came from the direction of the source. For every detected shower, then, the angular distance θ from the shower direction to the source is calculated (see Figure 8). Showers of small θ are more consistent with having originated at the source.

In order to filter out hadronic background, we reject those shower events that do not pass certain image dimension criteria, or *cuts*. The two main cuts employed in preferentially selecting gamma-ray events are *Mean Scaled Length* (MSL) and *Mean Scaled Width* (MSW). The MSL of a shower event is defined as

$$MSL = \frac{1}{N_{tel}} \sum_{i=1}^{N_{tel}} \frac{\ell_i}{\langle \ell \rangle_i} \tag{8}$$

where ℓ_i is the length of the image (calculated as described above) in the ith telescope, and $\langle \ell \rangle_i$ is the expected value for the length of the image in the ith telescope. The parameter $\langle \ell \rangle_i$ is determined by simulations, and depends on both the distance of the core position from the ith telescope's position on the ground and the size of the image in the ith telescope. MSW is defined analogously.

In filtering out shower images that fail to pass the cuts, inevitably some gamma-ray showers are rejected and some hadronic showers are selected. Using simulations, one can create a set of cuts that maximize the signal-to-noise ratio. The cuts used in the following observations, the most important of which are the MSL and MSW cuts, are listed in Table 2.

3.5. Wobble Analysis

From the reconstructed shower direction of each of the selected events, a sky map of where the detected showers came from can be compiled. From this one can determine which events came from the direction of the source, or, more realistically, which events came from a region immediately around the source ($\theta < \theta_{cut}$). Denote the number of these events by N_{on}. In order to interpret this number, it is neccessary to estimate the number of events expected due to remaining cosmic ray background. Wobble analysis is one method developed to estimate this background. In wobble analysis, instead of pointing the telescope directly on the source, it is pointed at a slightly offset position (in this data usually $\pm 0.3°$ in either RA or Dec). To estimate the number of background events, background regions are defined at the same offset from the telescope tracking position (see Figure 10). The number of events in each of the background rings is averaged. This value, denoted N_{off} is the desired estimate of the background, so we can determine the excess number of events in the on-source region

$$N_{ex} = N_{on} - N_{off}. \tag{9}$$

The significance of this excess is determined using the maximum likelihood method described in Li & Ma (1983).

4. Results

The sky map of the selected reconstructed events can be seen in Figure 11. It is clear that a source is detected near the intersection of the crosshairs (the coordinates of Mrk 501). Using methods analogous to those described in section 3.3, the centroid of the sky map image was calculated to be at coordinates RA 253.467° Dec 39.795°, in agreement to within a couple of arcminutes with Mrk 501's coordinates RA 253.467° Dec 39.760° as taken from the NASA Extragalactic Database (http://nedwww.ipac.caltech.edu/). There were $N_{on} = 160$ on-region events, with an estimated background of $N_{off} = 75$ events. The excess $N_{ex} = 85$ events in the on-region has a significance of 7.57 σ. The distribution of this excess can be seen in the θ^2 distribution shown in Figure 12.

The average rate of excess gamma-ray detection throughout the nine night observation period was 0.13 ± 0.017 γ-rays min^{-1}, approximately 7% of that of the Crab Nebula. A night-by-night light curve can be seen in Figure 13. None of the flaring behavior seen previously for Mrk 501 is visible in our observations. Instead, the gamma-ray flux observed stays consistently at a low level, without much variation. A light curve at five minute intervals of the observations on April 26, 2006 is displayed in Figure 14. While, again, the observed rate

never exceeds even half of that from the Crab Nebula, we see that on timescales as short as five minutes the observed rate can vary from $\sim 10\%$ to $\sim 40\%$ of the Crab rate.

While the data set is too small to determine with any confidence the differential energy spectrum observed from Mrk 501, a primitive method can be used for determining the qualitative structure of the observed energy spectrum. By noting that the total size of the images in a shower event is roughly proportional to the energy of the primary gamma ray, a size distribution of the excess shower events should have the same functional form as the energy spectrum. Such a distribution is shown in Figure 15. The distribution has a roughly linear falloff on a logarithmic plot, which would imply a power-law differential energy spectrum. Such a spectrum has been previously observed, and is expected.

5. Discussion

A strong signal (7.57σ) was detected from Mrk 501 in a low emission state (0.13 γ-rays min^{-1}) with the VERITAS two telescope array after 11 hours of observation. The strength of this signal after only 11 hours is without parallel among the results of first-generation detectors prior to the 1997 flare, suggesting that the greater sensitivity of the VERITAS array is able to determine with far greater temporal resolution the low level emission spectrum of the blazar. This is supported by the fact that flux variations on timescales as short as 5 minutes are clearly visible in nightly observation data.

It is interesting to note that we observed an excess number of events at distances as far away as $\theta = 0.28°$ from Mrk 501. It is possible that some of these excess events fell within the background rings during the wobble analysis, overestimating the background. If this is the case, the observed significance should actually be greater.

These early results are promising for the new generation of Čerenkov imaging arrays, and for the VERITAS array in particular. With the greater sensitivity and collection area of an additional two telescopes, the low-level of emission from Mrk 501 should be obtained with greater accuracy, allowing for variations to be observed with better precision on short timescales (< 5 minutes). The qualititative structure of the size distribution obtained suggests that with this greater sensitivity a differential energy spectrum can be obtained for Mrk 501's low-level emissions. The spectral index of the power law spectrum in this base state can then be compared to that observed during periods of flaring.

6. Acknowledgements

REFERENCES

Aharonian, F. et al. 1997, A&A, 327, L5

—. 2005, A&A, 441, 465

Bradbury, S. M. et al. 1997, A&A, 320, L5

Catanese, M. et al. 1997, ApJ, 487, L143+

Davies, J. M., & Cotton, E. S. 1957, Journal of Solar Energy, 1

Holder, J. et al. 2006, Astroparticle Physics, 25, 391

Li, T.-P., & Ma, Y.-Q. 1983, ApJ, 272, 317

Punch, M. et al. 1992, Nature, 358, 477

Quinn, J. et al. 1996, ApJ, 456, L83+

—. 1999, ApJ, 518, 693

Rico, J., & the MAGIC collaboration. 2006, Journal of Physics: Conference Series, 39, 454

Table 1.   Markarian 501 Wobble Runs

Run Number	Date	Start Time	Duration (min.)	Offset[1] (°)
30483	04/26/06	09:11:10	28.00	-0.301 Dec
30484	04/26/06	09:40:24	28.00	0.301 Dec
30485	04/26/06	10:10:23	28.00	-0.298 Dec
30486	04/26/06	10:41:07	28.00	0.504 Dec
30487	04/26/06	11:10:15	16.65	-0.500 Dec
30498	04/27/06	09:05:38	28.00	0.296 Dec
30499	04/27/06	09:35:32	28.00	-0.299 Dec
30500	04/27/06	10:05:33	28.00	0.302 Dec
30501	04/27/06	10:35:08	18.93	-0.299 Dec
30602	05/03/06	08:37:11	28.00	0.300 Dec
30603	05/03/06	09:07:15	28.00	-0.300 Dec
30822	05/25/06	07:21:45	28.00	0.276 Dec
30863	05/27/06	08:12:37	29.98	0.306 Dec
30864	05/27/06	08:44:21	30.00	-0.299 Dec
30878	05/28/06	07:16:38	30.00	0.298 Dec
30879	05/28/06	07:50:34	30.00	-0.298 Dec
30897	05/29/06	07:59:25	28.00	0.310 Dec
30898	05/29/06	08:52:40	28.00	-0.300 Dec
30899	05/29/06	09:22:07	28.00	0.390 RA
30944	05/31/06	08:31:06	28.00	0.301 Dec
30945	05/31/06	09:01:06	28.00	-0.300 Dec
31117	06/19/06	06:10:21	28.00	0.301 Dec
31118	06/19/06	06:42:09	28.00	-0.298 Dec
31119	06/19/06	07:12:05	28.00	0.391 RA

[1]The wobble run offset is defined in section 3.5

Table 2.   Gamma-ray Selection Cuts[1]

Size	Distance	MSL	MSW	Number of Pixels
$S^0 > 500$ dc	$d \leq 1.5°$	$0.04 < \text{MSL} < 1.2$	$0.04 < \text{MSW} < 0.9$	$N_{px} \geq 4$

[1]These quantities are defined in sections 3.3 and 3.4

Fig. 1.— The first VERITAS telescope, at the VERITAS base camp at the Whipple Observatory in Southern Arizona. The completed VERITAS array will consist of four such telescopes.

Fig. 2.— Telescope Camera Box, located at the focus of the telescope reflector. In the center is a high resolution, 499 PMT camera. Taken from Holder et al. (2006).
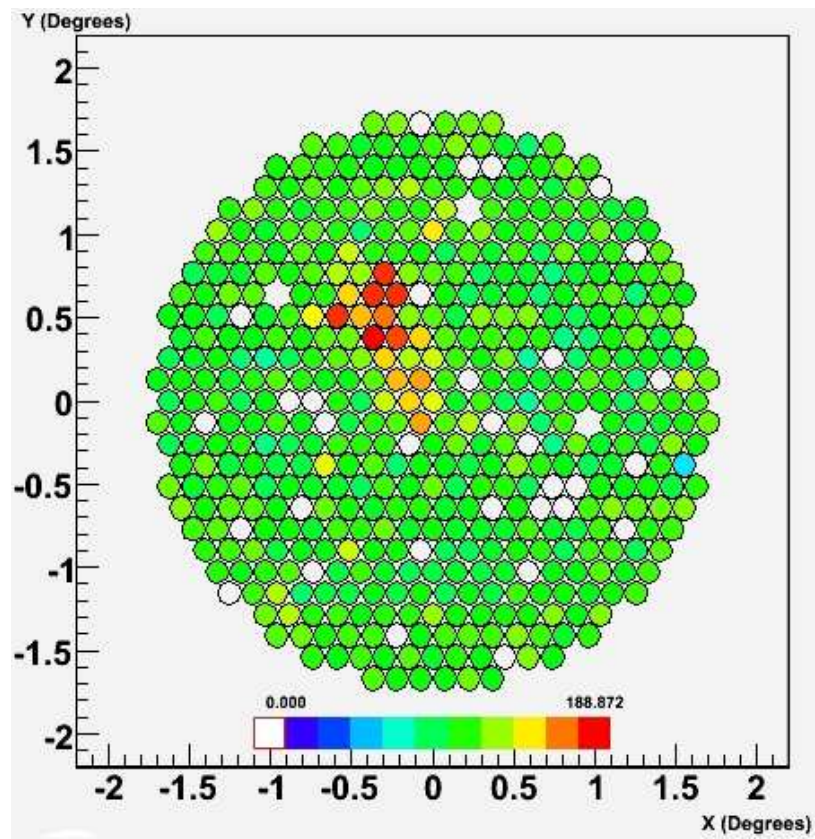
Fig. 3.— One γ-ray image stored during observation. The color levels denote the integrated charge of the pixel, in digital counts.
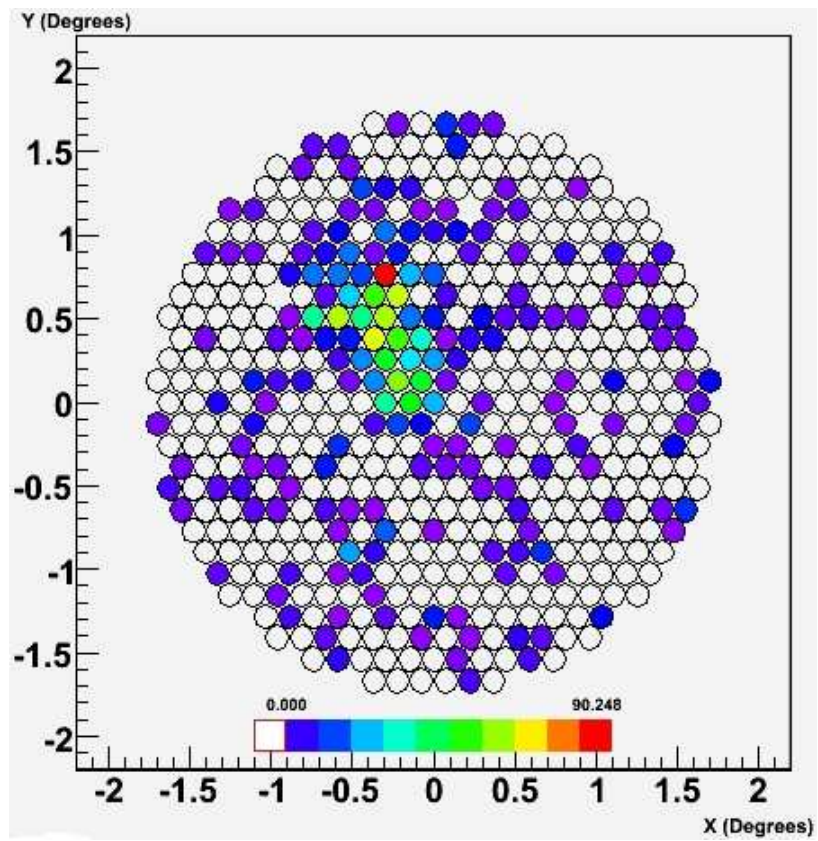
Fig. 4.— The same γ-ray image, after removing the DC pedestal.
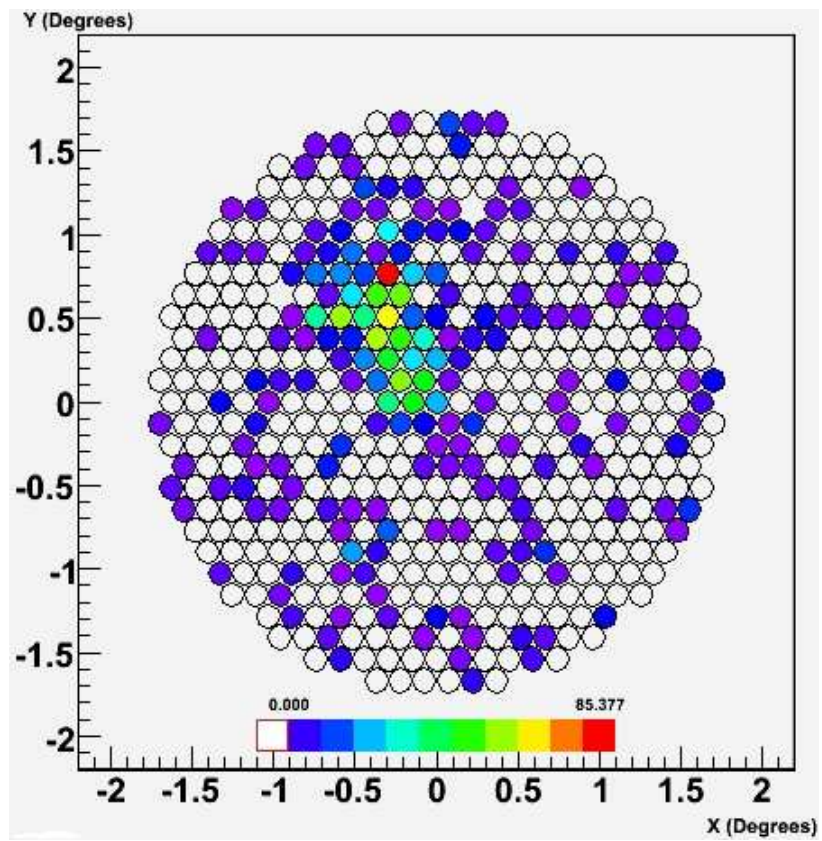
Fig. 5.— The same γ-ray image, after equalizing the PMT gains.
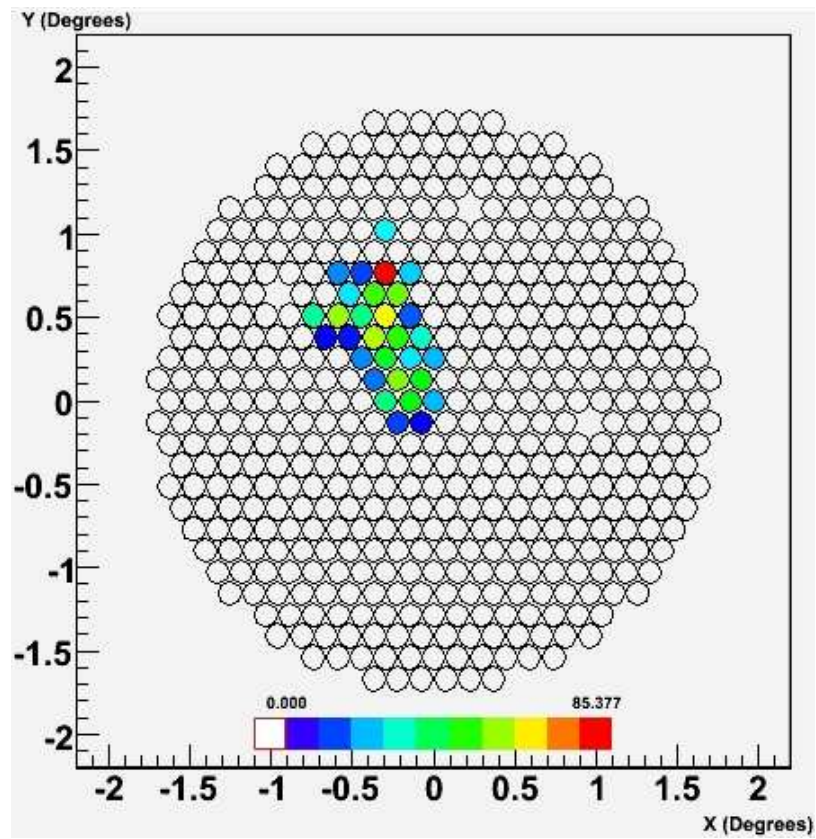
Fig. 6.— The same γ-ray image, after cleaning up the image to remove night sky noise.
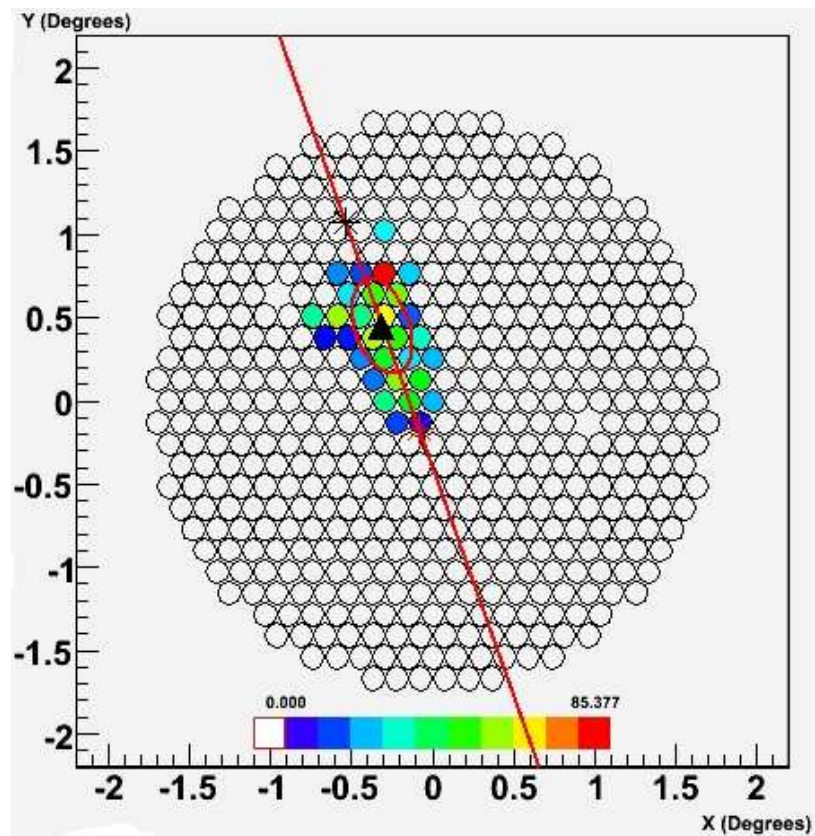
Fig. 7.— The result of parameterizing the same γ-ray image. Note that the shower image is compact and roughly elliptical, as is characteristic of γ-ray images.
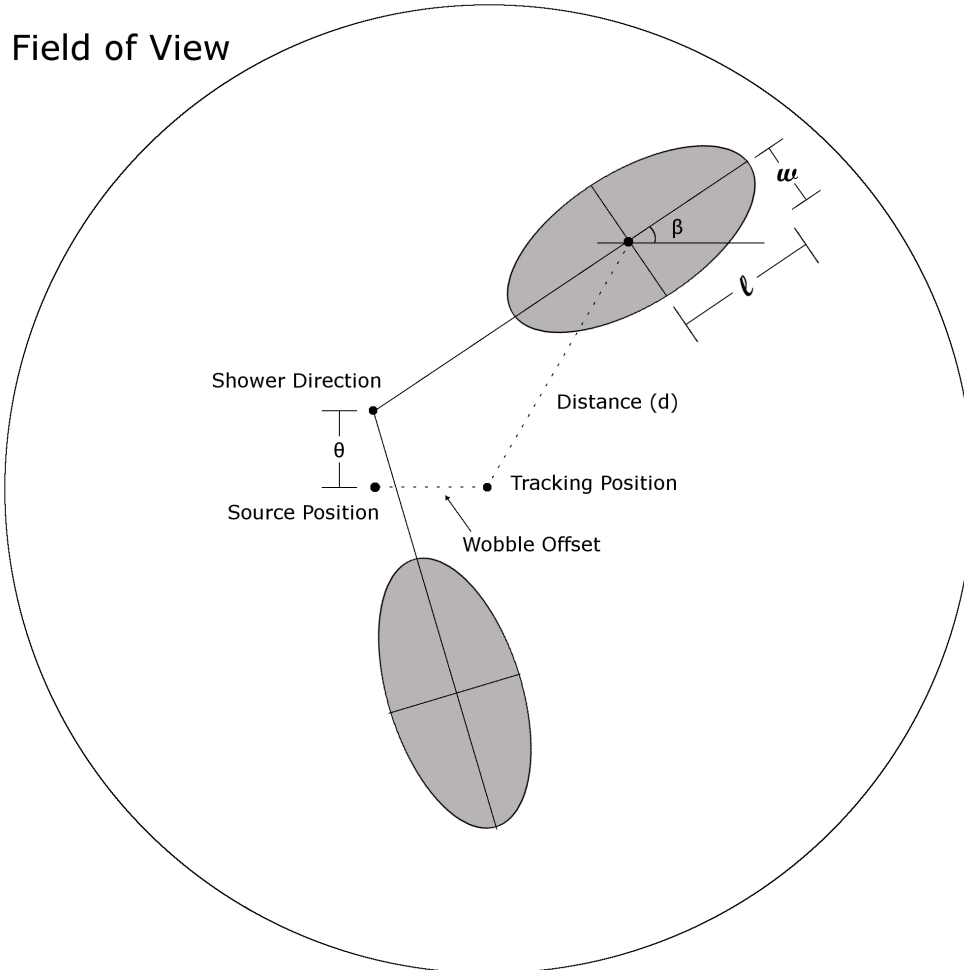
Fig. 8.— The parameters ℓ, w, β, and d as determined by the image parameterization. To reconstruct the shower direction, we take the intersection of the major axes of each of the image ellipses in each telescope. The parameter θ is the distance from this shower direction and the source position.

Ground
Coordinates

Core Position

Telescope 1   Telescope 2
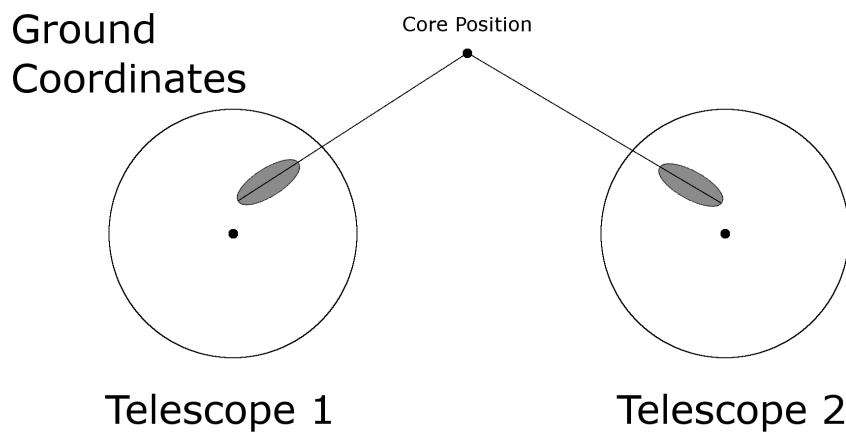
Fig. 9.— To reconstruct the core position, we take the intersection of the major axes of each of the image ellipses superimposed on the ground coordinate plane.
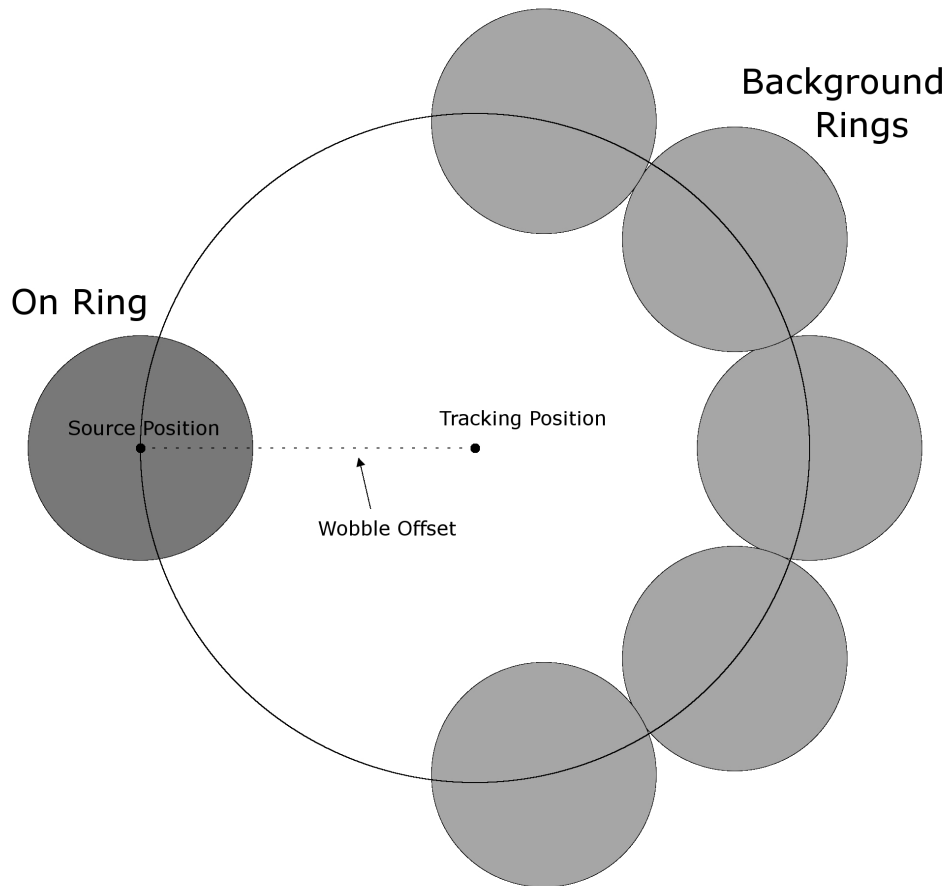
Fig. 10.— Wobble Analysis. Events falling within the on ring and the background rings are counted, and the excess number of events is determined.
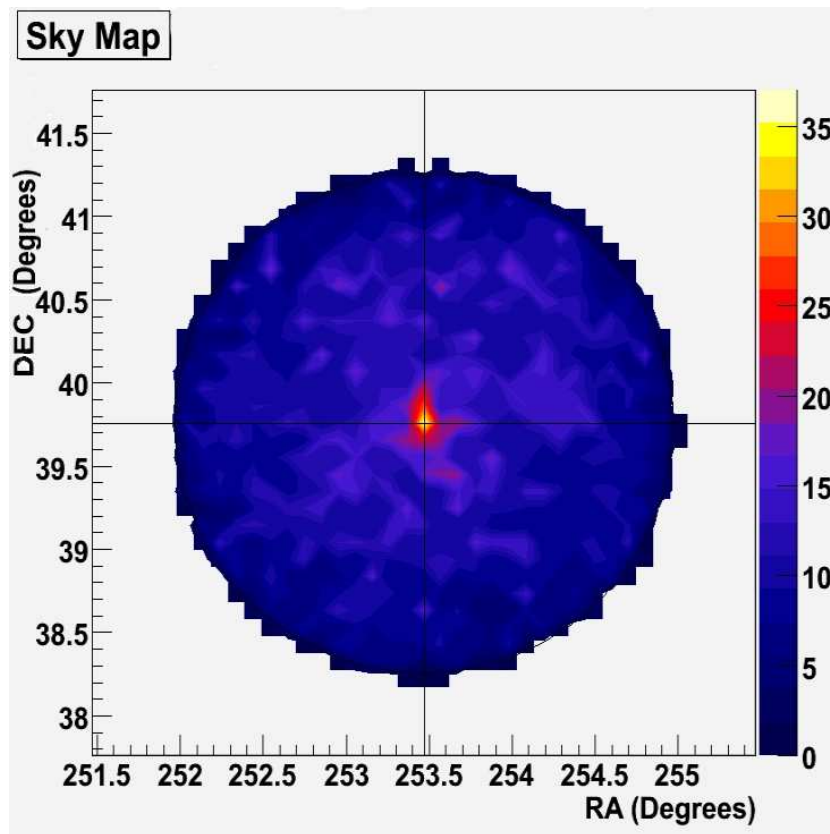
Fig. 11.— The sky map of all shower events that passed the selection cuts. The color corresponds to the number of these events coming from the particular region of sky.
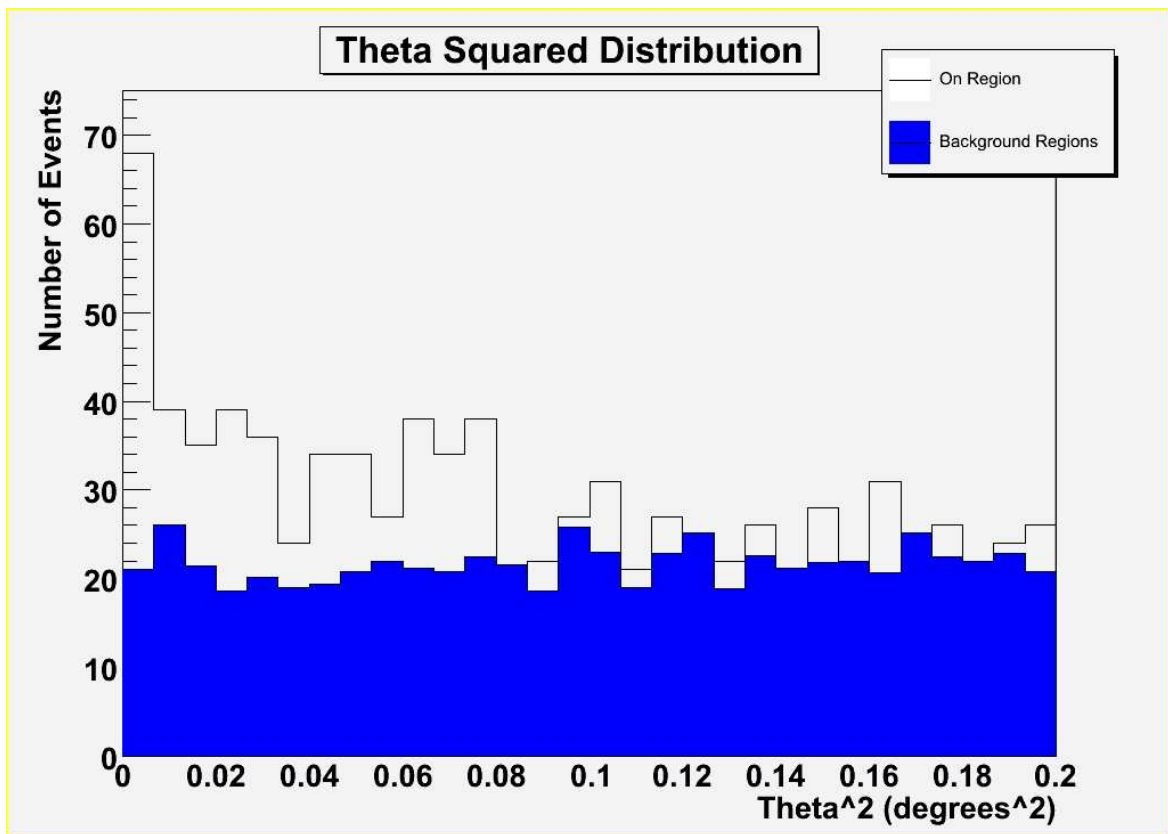
Fig. 12.— The theta-squared distribution for the Mrk 501 data. Theta is defined in Figure 8. A clear excess of events occurs at low values of theta-squared.
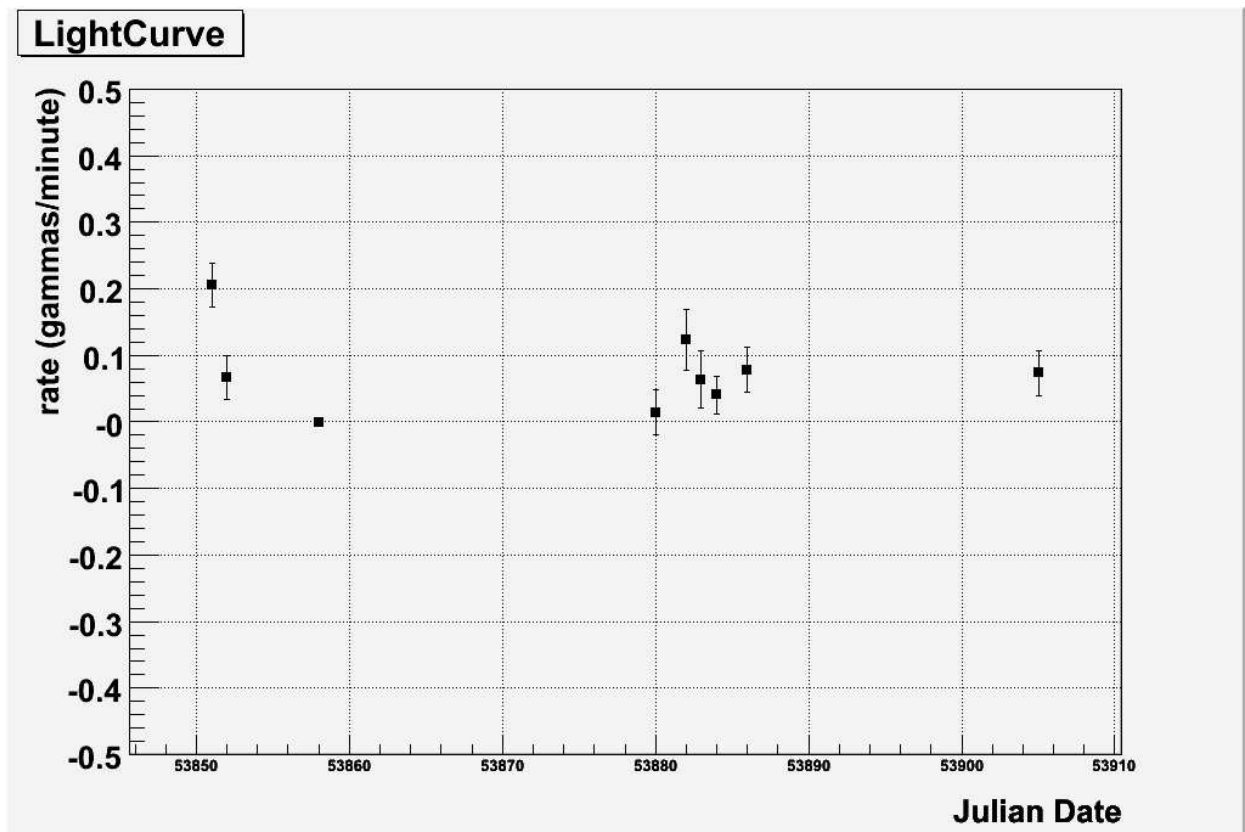
Fig. 13.— Nightly Light Curve. Each point is the rate of γ-ray detection for an entire night of observation (Spring 2006).
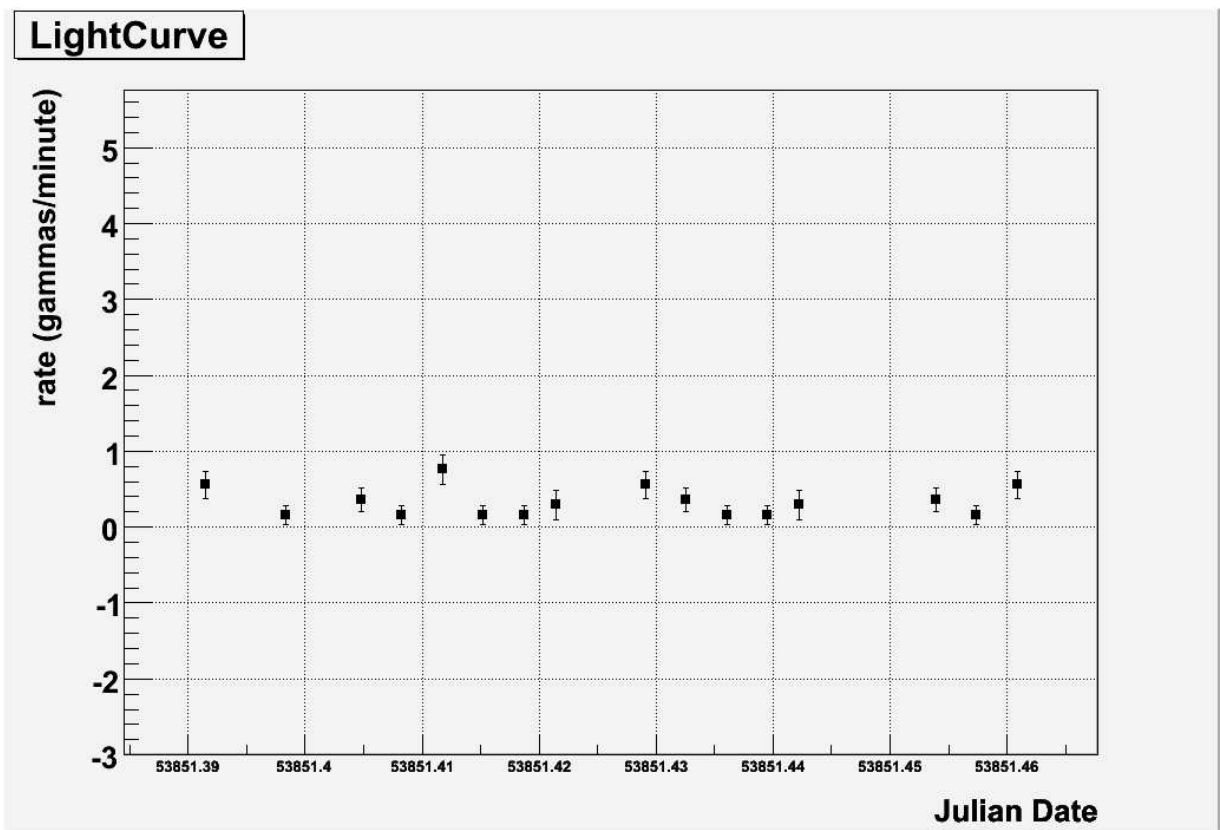
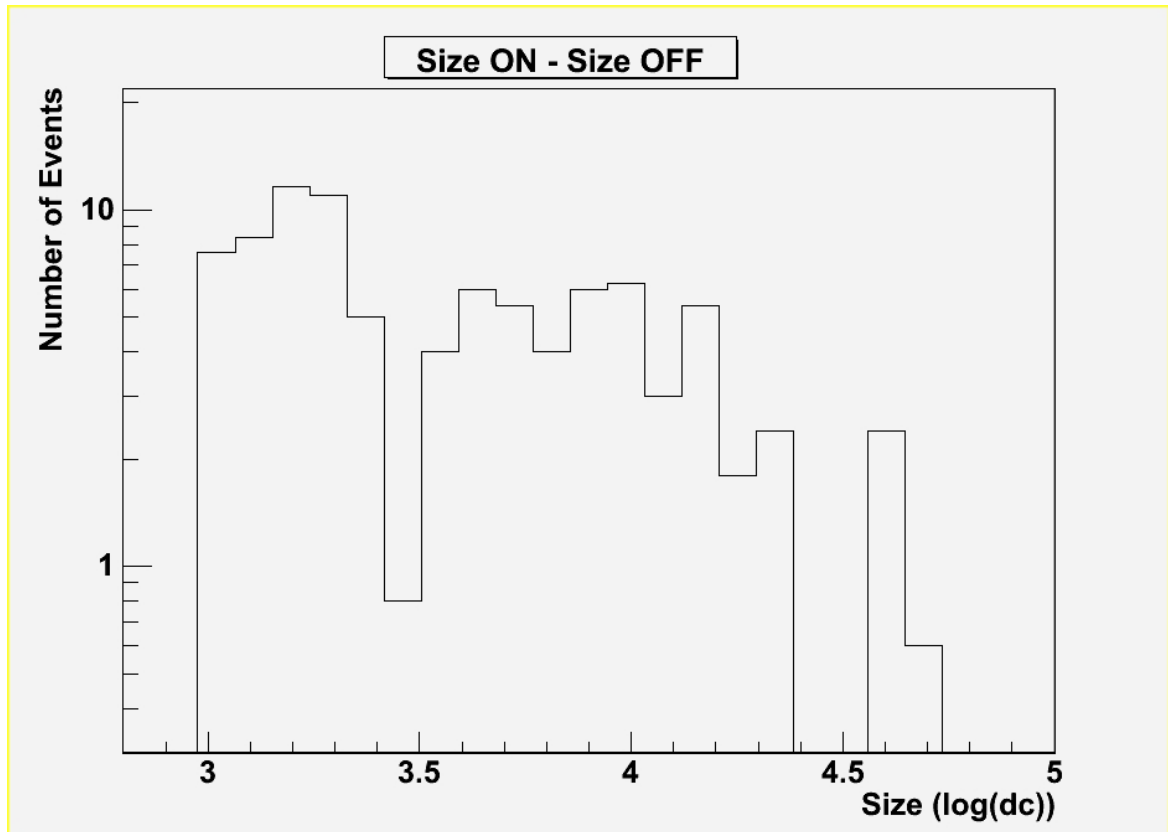Fig. 14.— Light curve for April 26, 2006. The interval between successive points is 5 minutes.

Fig. 15.— Difference between the size distribution of ON events and OFF events. Because the excess ON events are statistically indicative of the number of γ-rays observed, this plot shows the size distribution of the observed γ-rays.